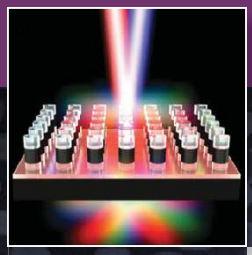

Nonlinear optics with resonant metasurfaces

Thomas Pertsch and Yuri Kivshar

The field of nonlinear optics is a well-established discipline that relies on macroscopic media and employs propagation distances longer than a wavelength of light. Recent progress with electromagnetic metamaterials has allowed for the expansion of this field into new directions of new phenomena and novel functionalities. In particular, nonlinear effects in thin, artificially structured materials such as metasurfaces do not rely on phase-matching conditions and symmetry-related selection rules of natural materials; they may be substantially enhanced by strong local and collective resonances of fields inside the metasurface nanostructures. Consequently, nonlinear processes may extend beyond simple harmonic generation and spectral broadening due to electronic nonlinearities. This article provides a brief review of basic concepts and recent results in the field of nonlinear optical metasurfaces.

Introduction

In recent years, metasurfaces have attracted a great deal of attention from the optics community as highly functional, broadband, and large-area structures for flat-optics components, which are rapidly advancing toward real applications. While the study of linear properties of metasurfaces is already being used in engineering, applications of nonlinear metasurfaces are just beginning to emerge. Detection and generation of light with new frequencies as well as generation and control of single photons for quantum information applications are significant for a range of modern technologies, and they drive research in nonlinear optical metasurfaces to improve both performance and functionalities of photonic devices.

In this article, we overview how nonlinear properties of metasurfaces can be engineered for applications. Multipolar interferences and enhanced local and collective resonances drive nonlinear light generation from nanoscale elements, with controlled direction of high-harmonic generation and frequency mixing. The nonlinear processes are empowered by the excitation of electric and magnetic Mie resonances (defined as localized solutions of Maxwell's equations for subwavelength particles) and their nonlinear material interaction, such as switching the phase of the fundamental and harmonic fields due to the nonlinear response of the component materials and precise control of structural dimensions at the nanoscale.

We concentrate on the most recent achievements in the field, which have been enabled by multiple advances to control light by nanostructured dielectric metasurfaces made from resonant structures and strongly nonlinear materials, (e.g., semiconductors or perovskites). In contrast to the long established field of metal-based plasmonic metasurfaces, their low-loss twin, the field of all-dielectric metasurfaces, has just emerged in the past few years. With respect to the many applications that enable the control of metasurface parameters, dielectric nanostructures fabricated from a multitude of high-index optical materials have already outperformed established metals in particular due to their considerably lower intrinsic losses.

Recently, research on dielectric metasurfaces has broadened to active[1] and nonlinear structured surfaces, where in addition to the low loss, the increased field overlap of the excited Mie-like resonances with the nonlinear dielectrics and the higher damage threshold became equally important. Though this field is relatively new, it has already attracted substantial attention, since it is expected to enable many advanced photonic applications in imaging, sensing, signal processing, and communication. There have been several recent reviews.[2–8]

Here, we concentrate on the major processes that enable this progress. We discuss recent new perspectives in materials, technologies, and applications. We start by introducing major linear resonance effects exploited to boost and control the

Thomas Pertsch, Friedrich Schiller University Jena, and Fraunhofer Institute for Applied Optics and Precision Engineering Jena, Germany; thomas.pertsch@uni-jena.de
Yuri Kivshar, The Australian National University, Australia; ysk124@physics.anu.edu.au
doi:10.1557/mrs.2020.65

nonlinear interactions. Driven by important novel functionalities of nonlinear metasurfaces (**Figure 1**), we describe recent achievements in realizing frequency conversion and high-harmonic generation. We close by reviewing recent demonstrations of nonlinear metadevices, realized by using nonlinear interactions, and finish with our viewpoint on the near-future directions for this field.

Resonances in metasurfaces

Resonances play a crucial role in the physics of metasurfaces because they allow substantial enhancement of both the electric and magnetic fields, which is an important requirement for nonlinear photonics. We can identify several physical mechanisms for the field enhancement and mode engineering in metasurfaces. This includes local resonances, such as surface plasmon resonances, Mie resonances of individual metallic and dielectric nanoparticles, and collective resonances such as guided-mode resonances, Fano resonances, and bound states in the continuum (BIC).

Surface plasmon resonance is the resonant oscillation of conduction electrons at the surface of a metallic nanoparticle separating negative (metal) and positive (air) permittivity materials stimulated by incident light. Such resonances are associated with strong localization of energy in subwavelength regions, but with strong absorption by the metal nanoparticles (typically gold or silver).

Mie resonances are associated traditionally with the exact Mie solutions of Maxwell's equations for spherical particles. In a broader context, they can be employed for the control of light below the free-space diffraction limit by high-index dielectric nanoparticles, and recently, they have attracted attention because they can support both electric and magnetic type resonances of comparable strengths.[14–16]

Fano resonance is a fascinating phenomenon of wave physics observed across various branches of optics, including photonics, plasmonics, and metamaterials.[17] Nanophotonics deals with extremely strong and confined optical fields at subwavelength scales far beyond the diffraction limit. Fano resonances arise from interference between different localized modes and radiative electromagnetic waves, and are supported by an appropriate combination of nanoparticles.[17] A Fano resonance typically manifests itself as resonant suppression of the total scattering cross section accompanied by enhanced absorption in nanophotonic structures and metasurfaces. Fano resonances confine light more efficiently and are characterized by a stronger dispersion (steeper wavelength dependence of scattering strength) than conventional resonances, which makes them promising for nanoscale biochemical sensing, switching, or lasing applications.

All such resonances, including surface plasmon resonances, Mie resonances, and Fano resonances, can be found in many systems that include a few nanoparticles, either metallic or dielectric, and they can be excited and observed in dimers and in clusters of metallic and dielectric nanoparticles called oligomers. Compared to plasmonic oligomers, all-dielectric structures are less sensitive to the separation between the particles, since the field is localized mainly inside the dielectric nanoparticles.[18] Moreover, since dielectric nanostructures exhibit almost negligible losses, they allow the observation of Fano resonances for new geometries not supported by their plasmonic counterparts. These novel features lead to different coupling mechanisms between nanoparticles making all-dielectric oligomer structures attractive for applications in active nanophotonics.

Arrays of nanoparticles composed into metasurfaces demonstrate richer classes of optical resonances. First, metasurfaces demonstrate resonances based on the resonances of individual nanoparticles, such as mirror-like reflectors for electromagnetic waves.[19] In addition, nanoscale-patterned surfaces and films with subwavelength periodicity sustain novel collective resonance effects when the input light couples to leaky waveguide modes.

These resonances were first suggested for diffractive gratings and termed "guided-mode resonances"[20] to reflect the fundamental physics governing these phenomena. They were previously termed "anomalous modes" in the scattering of light. In recent years, such phenomena are associated with metasurfaces. Nevertheless, the resonance physics does not depend on the structure's periodicity only in a fundamental way. Various spectral expressions

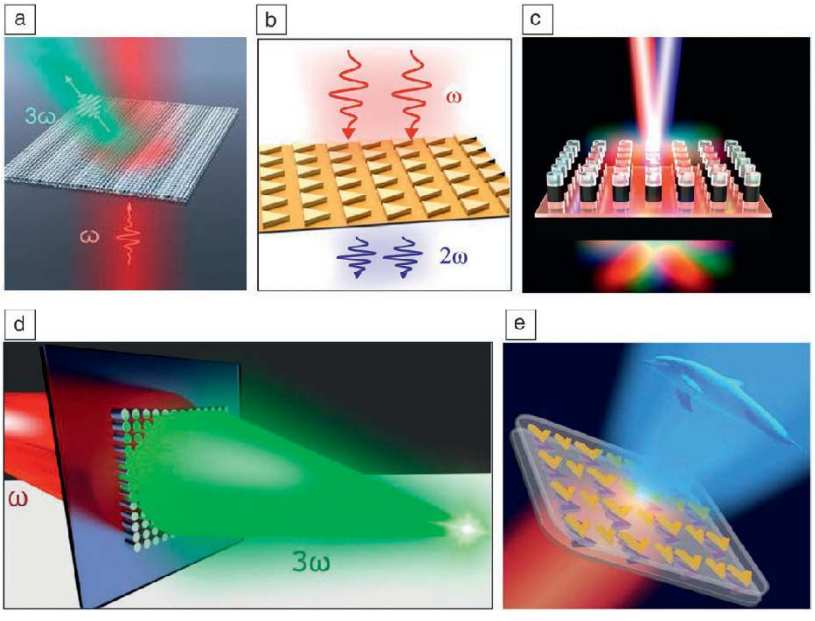

Figure 1. Select examples of useful functionalities of nonlinear metasurfaces. (a) Third-harmonic generation with nonlinear beam deflection,[9] (b) resonant second-harmonic generation,[10] (c) two-beam frequency mixing,[11] (d) nonlinear metalens,[12] and (e) nonlinear hologram.[13] Note: ω, frequency of exciting light.

are available with wide parametric design spaces to control the amplitude, phase, polarization, near-field intensity, and light distribution on metasurfaces as generalized periodic media.

Periodic media exhibit interesting properties, also supporting both leaky edge and non-leaky edge modes for each supported resonant Bloch wave (as extended wave solutions of periodic potentials) if the lattice is symmetric. The non-leaky edge is associated with a BIC, or an embedded eigenvalue, which is of considerable scientific interest because it can provide a physical mechanism for trapping electromagnetic energy for a long time.[21,22] A true BIC is a mathematical object with an infinite value of the resonance spectral width, often called the quality factor (Q factor). In practice, BIC can be realized as quasi-BIC, being directly associated with the so-called supercavity mode,[23] where both the Q factor and resonance width become finite. Nevertheless, BIC-inspired localization of light makes it possible to realize high-Q quasi-BIC modes in conventional optical structures such as optical cavities, photonic-crystal slabs, and coupled optical waveguides.

It has been shown recently that the resonant response of dielectric metasurfaces composed of resonators (often called "meta-atoms") with broken in-plane inversion symmetry can support high-Q resonances directly associated with the concept of the BIC.[24] This includes, in particular, broken-symmetry Fano dielectric metasurfaces for enhancement of nonlinear effects[25] and reported sensing with pixelated dielectric metasurfaces.[26] All such structures can be employed in nonlinear nanophotonics, since they give rise to strong light–matter interaction on the nanoscale. It was shown that an asymmetry induces an imbalanced interference between counter-propagating leaky waves comprising a BIC that leads to radiation leakage.[21] Similarly, breaking the symmetry transversely, in the direction perpendicular to a metasurface, with a complex unit cell allows control of the number, frequency, and type of high-Q resonances originating from the BIC physics.

Figure 2 shows the concept of quasi-BIC modes in plasmonic or dielectric metasurfaces with broken in-plane symmetry. Figure 2a schematically shows a metasurface composed of a square lattice of pairs of dielectric bars of different widths, but many other types of meta-atoms are available, as shown in Figure 2b. Importantly, all such metasurfaces are characterized by the inverse quadratic dependence of the radiative Q factor on an asymmetry parameter α, as was first proven analytically (Figure 2c).[24]

A direct link exists between quasi-BIC states and Fano resonances because these two phenomena originate from similar physics. It has been shown[24] that the transmission spectra of dielectric metasurfaces with broken symmetry near the condition of the quasi-BIC resonance can be described explicitly by the classical Fano formula, and the observed peak positions and linewidths correspond exactly to the real and imaginary parts of the eigenmode frequencies. The Fano parameter becomes ill-defined at the BIC condition, which corresponds to a collapse of the Fano resonance.[27] Importantly, every quasi-BIC mode can be linked with a Fano resonance, whereas the opposite is not true—a Fano resonance may not converge to a BIC mode for any variation of the system parameters.

Figure 3 shows several examples of dielectric metasurfaces supporting quasi-BIC resonances, shown as scanning electron microscope images of the fabricated structures. Such metasurfaces have the potential to significantly improve optical sensing applications as well as to increase the efficiency of integrated light sources. Figure 3a presents a part of a Si metasurface with the highest value of the Q factor demonstrated so far, with Q = 18,511.[28] Figure 3b shows a Ge-based high-Q metasurface capable of delivering a multitude of spectrally selective and surface-sensitive resonances between 1100 and 1800 cm^{-1} for detecting distinct absorption signatures of different interacting analytes including proteins, aptamers, and polylysine.[29] Finally, the example in Figure 3c shows a light-emitting metasurface that combines an asymmetric Si nanorod array with Ge quantum dots embedded directly in the Si nanorods. For the last metasurface (Figure 3c), the authors observed light emission intensity enhancement and specific polarization of far-field radiation driven by symmetry-breaking-induced Fano resonances.[30]

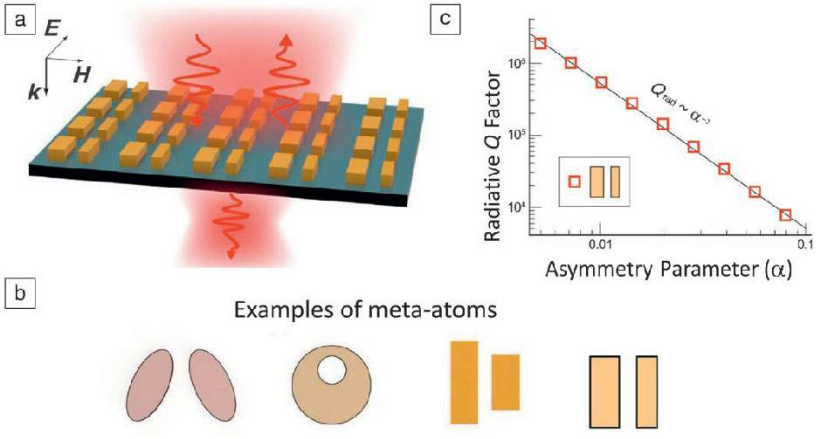

Figure 2. The concept of quasi-bound states in the continuum modes in dielectric metasurfaces with a broken in-plane symmetry. (a) Schematic of the scattering of light by an asymmetric metasurface composed of a square lattice of pairs of dielectric bars of different widths. (b) Examples of asymmetric meta-atoms. (c) Inverse quadratic dependence of the radiative Q (quality) factor on the asymmetry parameter α (log-log plot). The inset shows the specific shape of the isolated asymmetric meta-atom. Adapted with permission from Reference 24. © 2018 American Physical Society. Note: Q_{rad}, radiative quality factor; E, electric field; H, magnetic field; k, wave vector.

Frequency conversion in nonlinear metasurfaces

Resonant excitations in metasurfaces, the different types of which were discussed in the previous section, boost light–matter interactions. Due to resonant field enhancement inside

dielectric nanostructures, nonlinear light–matter interactions can occur for easily accessible excitation intensities. However, besides the onset of nonlinear effects for reduced excitation powers and the increased damage threshold as compared to metal nanostructures, dielectric metasurfaces offer multiple additional advantages for the generation, control, and exploitation of nonlinear optical effects. These advantages, similar to field enhancement, derive from resonant excitations in the thin nanostructured films of dielectric metasurfaces.

The following specific properties can be discussed:

1. Phase matching: The thin-film nature of metasurfaces, with thicknesses smaller than the wavelength of light, resolves any phase-matching issue, which otherwise often hampers nonlinear effects in macroscopic waveguide devices or bulk crystals. The reduced nonlinear efficiency, a consequence of the strongly decreased interaction length in thin metasurfaces, can at least partially be compensated by the discussed resonant field enhancement.
2. Field overlap: Since electromagnetic fields can penetrate into dielectric materials, there is strong overlap of resonantly excited modes with the nonlinear material of the dielectric nanostructures composing the metasurfaces. In contrast to plasmonic nanostructures, where the field is enhanced mainly at the surfaces of the nanostructures, this improved overlap gives rise to high nonlinear interaction efficiencies of dielectric metasurfaces. This overlap is often strongest for higher-order resonances (e.g., magnetic dipole resonances).
3. Symmetry breaking: While many nonlinear interactions, which are present on the microscopic level, do not result in macroscopic effects due to their suppression by symmetries of the materials and fields, nanostructured dielectrics can break the symmetry of both the materials on a nanoscopic level and the fields. The surface-to-volume ratio is enhanced for nanostructures, strengthening nonlinear surface effects. This can be enhanced further by breaking the nanostructures symmetries on the nanoscale. Moreover, compared to the trivial vectorial orientations of electromagnetic fields in bulk media, the hybridization of fields for higher-order modes in high-index dielectric nanostructures can be the origin of nonlinear interactions, which are symmetry-forbidden in bulk media.
4. Dispersion: Resonant interactions, as they occur in dielectric metasurfaces, are inherently dispersive in that they show different behaviors for different excitation frequencies. While this can often be a concern, due to the obstruction of broadband operation or induction of phase-mismatch in nonlinear frequency generation, we assume the perspective that this is a versatile feature, which should be used to tailor nonlinear interactions. By providing almost arbitrary control over the frequency dependence of the density of states in resonant dielectric metasurfaces, higher-order nonlinear frequency generations can be tailored at will or short pulses can be nonlinearly reshaped simply by controlling the linear dispersion properties of metasurfaces.
5. Spatial tailoring: Since the resonant properties of nanostructured metasurfaces depend strongly on the geometry of the nanostructures, the resonances can be spatially varied by varying the nanoscale geometries across the metasurfaces. While the nonlinear properties of bulk media are spatially homogeneous, this tailorability of the nanostructures allows tuning the linear and nonlinear properties across the metasurfaces, the interplay of which can be exploited for complex spatiotemporal nonlinear beam shaping and control.

The following is an overview of the demonstrated nonlinear frequency conversion processes by subdividing the field into second-harmonic generation (SHG) and third-harmonic generation (THG).

SHG

SHG, the creation of one high-energy photon (at the so-called second-harmonic [SH] frequency) from two low-energy photons (at the so-called fundamental harmonic [FH] frequency) of a single excitation beam, is a second-order nonlinear optical process. On the molecular level, it is the strongest nonlinear process when compared to higher-order nonlinearities. However, second-order nonlinear effects are often suppressed on the macroscopic scale by the centrosymmetry or amorphous character of most materials, by which the second-order nonlinear response of an atom or molecule is annihilated. Moreover, on the macroscopic scale, the dispersive nature of the material's response gives rise to different phase velocities of FH and SH waves by which they accumulate a phase difference during propagation. This effect, which is frequently referred to as phase mismatch, leads to destructive interference of SHG over macroscopic propagation distances and limits its efficiency.

Bulk crystal or waveguide techniques such as birefringent phase matching or quasi-phase

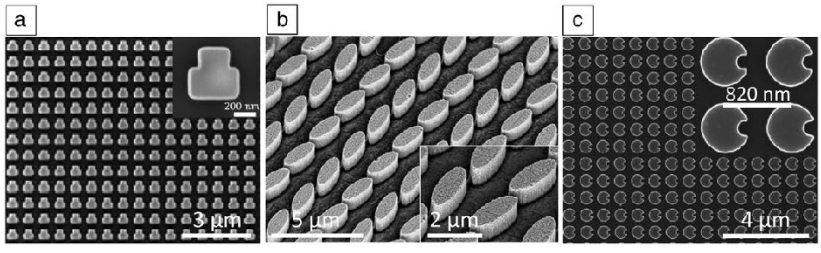

Figure 3. Examples of metasurfaces with broken in-plane symmetry supporting quasi-bound states in the continuum resonances, shown as scanning electron microscope images of the fabricated structures. (a) Silicon metasurface demonstrating the highest values of the quality factor,[28] (b) the structure of one pixel of the pixelated germanium metasurface employed for biosensing,[29] and (c) silicon metasurface with Ge quantum dots embedded in the silicon nanostructures showing enhanced light–matter interaction.[30] Insets show enlarged parts of the scanning electron microscope images.

matching have been developed to counteract the destructive effect of dispersion in SHG, the subwavelength thickness of metasurfaces renders phase mismatch irrelevant. Moreover, the microscopic centrosymmetry of materials can be broken on the nanoscale by the nanopatterning in metasurfaces, giving rise to SHG in materials, which would be symmetry-forbidden in their bulk form.

SHG was investigated in non-centrosymmetric metal nanostructures early in the development of plasmonic metasurfaces.[31,32] These plasmonic implementations of the metasurface suffered from intrinsic losses of metals and from their relatively low damage thresholds induced by these losses due to heating of the nanostructures. This latter fact, in particular, limits the applicability of nonlinear applications due to the power dependence of SHG efficiencies. It has been shown that by switching to dielectric metasurfaces, nonlinear efficiencies could be considerably boosted. This was discussed first for optomechanical nonlinearities,[33] and soon after, second-order optical nonlinearities with SHG were proposed.[34] Due to challenges in the large-scale fabrication of nanostructures from non-centrosymmetric crystalline materials, some of the research focused on single nanostructures, acting as nonlinear antennas.[35–41] These resonant nanostructures were made from second-order nonlinear crystals, including SiC,[35] AlGaAs,[36–38,40] ZnO,[39] and GaAs,[41] where the work from Reference 41 had been solving existing directionality problems of SHG by using (111)-grown crystals instead of previously used (100) crystals. In some of these studies on nonlinear antennas, entire arrays of antennas were fabricated and characterized to increase the detected SHG signal by collecting the nonlinear response of several antennas at once. Since these works focused on the dynamics of the isolated antennas while disregarding collective effects, they have not been considered as metasurfaces.

Eventually, the realization of real metasurfaces with densely arranged nanoparticles (as shown in the examples of **Figure 4**) concentrated on III–V semiconductors with high second-order nonlinearities, GaAs[42–44] and AlGaAs.[45,46] In these metasurfaces, SHG efficiency was increased as compared to homogeneous films by a factor of 10^4, initially by exploiting magnetic dipole resonances in symmetric nanoresonators,[42] but later, an even higher efficiency (enhanced by a factor of 13 as compared to GaAs nanodisks) was obtained by Fano resonances in broken symmetries.[43] Frizyuk et al.[47] recently discussed how symmetries of the resonances interacting with the symmetries of complicated nonlinear tensors in such III-V semiconductor nanoresonators can be exploited for efficient nonlinear processes.

Due to the small energy gap of III-V semiconductors, they are limited to SHG in the near infrared spectrum or otherwise

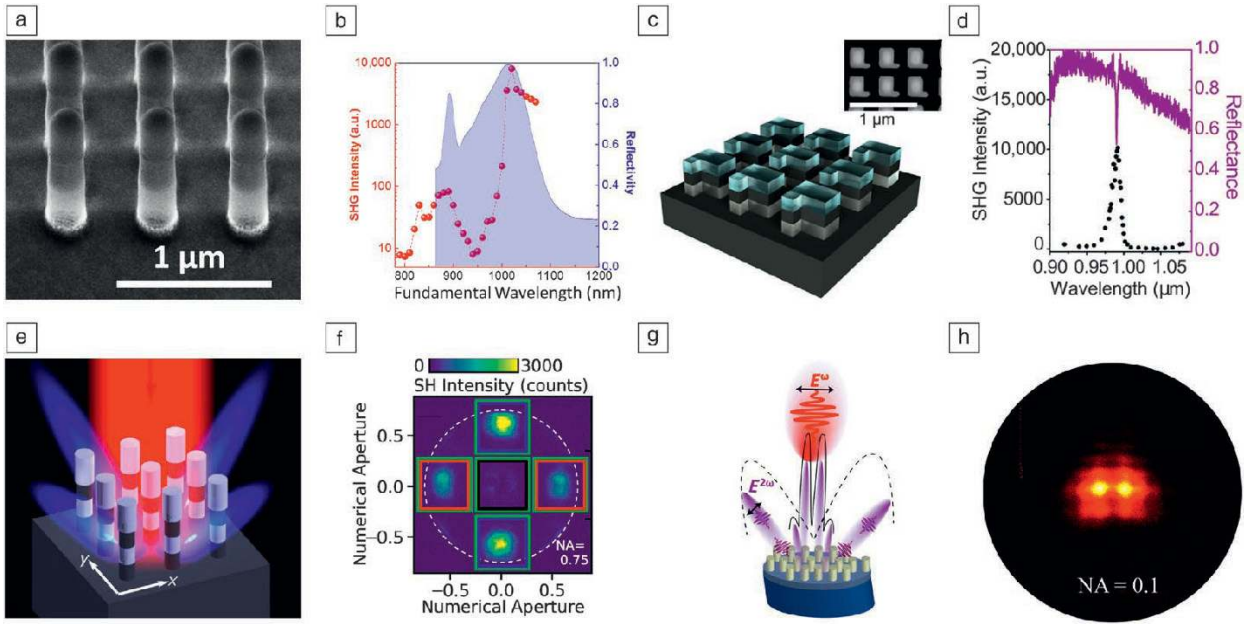

Figure 4. Second-harmonic generation (SHG) in III–V semiconductor metasurfaces with different geometries for exploiting specific resonance schemes and for controlling the angular emission spectrum of the second harmonic (SH). (a) By employing the magnetic dipole resonance in a GaAs metasurface illustrated by its scanning electron microscope image, strong SHG from bulk and surface nonlinearities is observed in (b) with 10^4 enhancement with respect to an unpatterned GaAs film.[42] (c) Utilizing Fano resonances in broken symmetry GaAs metasurfaces (inset shows the scanning electron microscope image of the structure), SHG could be resonantly enhanced by a factor of 13 with respect to GaAs nanodisks, as plotted in (d).[43] (e) Interference of electric and magnetic dipole resonances in a GaAs metasurface gave rise to SH emission into different diffraction angles plotted in (f) for an excitation wavelength of 890 nm.[44] (g) Modulation of Mie resonances via Bragg scattering at both fundamental and second harmonics in an AlGaAs metasurface was exploited to enable paraxial SHG into the zero order, as demonstrated by the measured angular spectrum in (h).[45] Note: NA, numerical aperture; $\boldsymbol{E}^{\omega}$, electric field at fundamental frequency; $\boldsymbol{E}^{2\omega}$, electric field at second-harmonic frequency.

suffer from absorption. Ferroelectrics such as lithium niobate and barium titanate have been explored for realizing nonlinear metasurfaces and nanoresonators, with applications in the visible or even ultraviolet spectrum.[48–53] Due to the lower ε of these ferroelectrics as compared to III–V semiconductors, the *Q* factor of the resonances and the achieved SHG efficiencies were quite low. In some studies, this was mitigated by hybridizing the ferroelectric nanoresonators with plasmonic nanoresonators to increase the field enhancement.[48,50]

Alternative realizations of metasurfaces and isolated nanoresonators were based on centrosymmetric materials, such as amorphous selenium,[54] (001)GaP,[55] nanocrystalline Si,[56] and amorphous Si.[57] To induce the normally symmetry-forbidden second-order nonlinear response from these nanostructures, the symmetry breaking property from the previous discussion was exploited using geometric symmetry breaking either at the surfaces or at the nanocrystal boundaries in the nanoresonators.

THG

THG, the creation of one high-energy photon (at the so-called third-harmonic [TH] frequency) from three low-energy FH photons of a single excitation beam, is a third-order nonlinear optical process. On the molecular level, it is weaker than the previously discussed second-order nonlinearity. However, unlike second-order nonlinear effects, third-order effects do not require non-centrosymmetry and are observed on a macroscopic scale (length scales comparable to or larger than the wavelength) for all materials. Therefore, the widely available Si, and to a lesser extent Ge, became the materials of choice for the realization of THG in metasurfaces. While the findings from symmetry breaking have not been considered for the nonlinear properties, all other arguments remain equally important for THG. Due to the large frequency shift from FH to TH, dispersion in resonant metasurfaces becomes more important for THG than for SHG.

Similar to SHG, the basic effects of THG in resonant dielectric nanostructures have been studied in isolated nanoantennas of Si[58] and Ge.[59] Also similar to SHG, it was discovered that magnetic dipole modes should be favored against electric dipole modes, because of their better field overlap with the nonlinear medium and the higher *Q* factor.[58,60] Further improvement of THG efficiency was achieved by increasing the *Q* factors based on the excitation of the hybrid superposition of the dipole and toroidal modes (often called "anapole modes") in Ge nanoresonators[59] and by increasing the field concentration based on hybridization of Si nanoresonators with plasmonic gold structures.[61]

Due to the maturity of Si nanofabrication, an understanding of THG in isolated Si nanoantennas could be realized in large-scale metasurfaces,[10,28,62–66] as summarized in **Figure 5**. Based on the high precision of Si nanofabrication, complicated geometries can be fabricated, with the well-established Mie-like resonances of the individual nanoresonators giving rise to collective resonance effects, such as Fano resonances,[62] BIC,[10,28] and topologically protected states.[66] Makarov et al. demonstrated an alternative to nanofabrication by electron-beam lithography by using self-adjusted laser lithography for

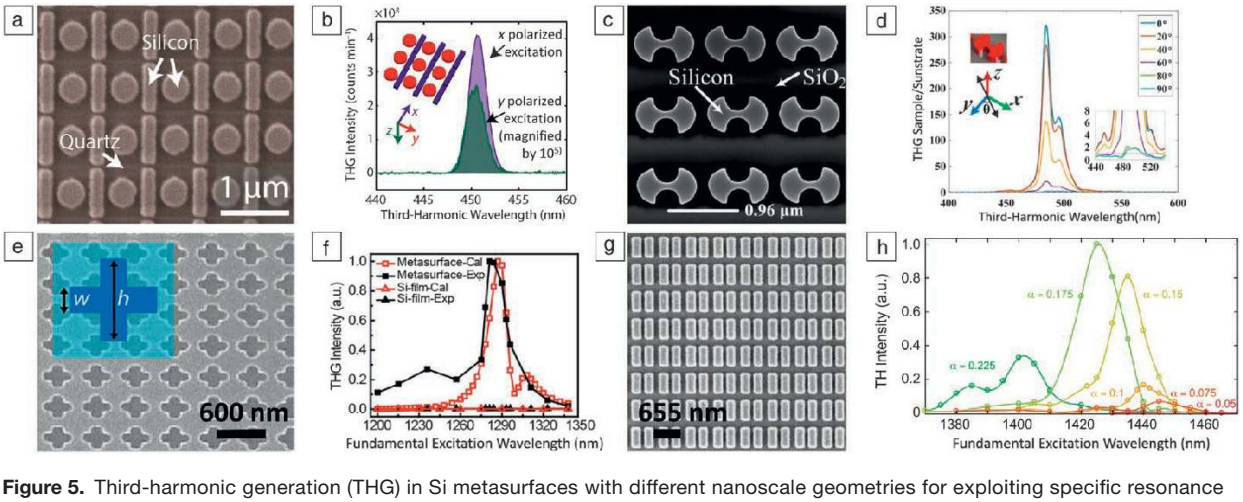

Figure 5. Third-harmonic generation (THG) in Si metasurfaces with different nanoscale geometries for exploiting specific resonance schemes. (a) Utilizing a Fano-resonant Si metasurface illustrated by its scanning electron microscope image, strong near-field enhancement resulted in strongly polarization dependent THG, seen by the strongly different THG intensity spectra plotted in (b) with 1.5×10^5 enhancement compared to an unpatterned Si film.[62] The inset in (b) illustrates the polarization orientation of the excitation. (c, d) By employing trapped modes in spindle-shaped Si nanoparticles, the THG could be resonantly enhanced by a factor of 3×10^2. (c) Scanning electron microscope image of the Si nanostructures. (d) Polarization dependent measured THG spectra. The upper left inset illustrates the polarization orientation of the excitation with respect to the spindle-shaped Si nanoparticles.[63] (e) Multipolar interference in cross-shaped nanoscale apertures in Si thin films gave rise to THG plotted in (f) with 10^2 enhancement compared to the unpatterned Si film, where the measured THG ("Exp") agrees well with calculations ("Cal").[65] (g) Bound states in the continuum and critical coupling were systematically studied for their THG enhancement (h) depending on the asymmetry parameter α, which characterizes the geometrical asymmetry of the employed Si double bar structure by determining the relative width reduction of the thinner silicon bar as compared to the thicker bar.[10]

writing nanostructures, potentially allowing for inexpensive large-scale fabrication.[64] Besides studying THG in metasurfaces, which consist of a large number of nanoresonators, some work also concentrated on exploring the effects arising from the transition from single dielectric resonators to oligomers that consist of a small number of dielectric nanoresonators.[67–69] Many of the resonance effects in metasurfaces have already been observed in oligomers, due to the interaction of three or four resonators.

High-harmonic generation and frequency mixing

High-harmonic generation (HHG) was first reported for rare gas atoms and was considered as one of the fundamental processes in strong-field physics and attosecond photonics.[70] Recently discovered HHG in solids[71] provides a new way to investigate novel strong-field photonic applications that cannot be realized in gases. In particular, this suggests the possibility of generating and controlling the high harmonics directly from subwavelength nanostructures. The effect of nanostructures on solid-state HHG is twofold—first, each individual nanoscale feature interacts with and scatters fundamental light in a nontrivial way depending on its geometry. Second, HHG emission profiles in the far field can be controlled by arranging the location of individual nanostructures.

All-dielectric resonant metasurfaces provide an attractive platform to control HHG and other high-field processes at the nanoscale. As previously discussed, by using collective resonances in metasurfaces, one can enhance the harmonic emission by several orders of magnitude compared to unpatterned samples. Liu et al.[72] employed a Fano-resonant Si metasurface[62] consisting of nanodisks and nanobars on a sapphire substrate (**Figure 6**a [inset]) and observed enhanced and highly anisotropic HHG that was selective to the excitation wavelength due to its resonant features. When the metasurface was resonantly excited, the high-harmonic signal was orders of magnitude higher compared to an unpatterned Si film at moderate driving intensities. Figure 6a shows the high-harmonic spectrum produced by the metasurface at an incident excitation intensity of 0.071 TW cm^{-2}. When the fundamental field is polarized along the nanobars, odd harmonics from the fifth to 11th are observed (solid red line), while no harmonics higher than the fifth are observed in unpatterned Si (dotted black line). At this intensity, the fifth harmonic is enhanced by the nanostructured metasurface by a factor of 30 compared to the unpatterned film, even though only the zero diffraction order is collected and the total area of structured Si is only 47% of the unpatterned film under the same illumination spot. The lower bound conversion efficiency for the fifth harmonic generated from the metasurface can be estimated as ~5 × 10^{-9} at an excitation intensity of 0.07 TW cm^{-2}. When the polarization of the excitation pulse is perpendicular to the nanobars, a configuration in which the bars' dipolar resonance is not excited, only the fifth and seventh harmonics are observed (solid green line). In this case, the yield for the fifth harmonic is similar to the unpatterned film and only a weak seventh harmonic is seen above the noise level, but reduced by a factor of 12 compared to the same harmonic yield in the parallel configuration.

Metasurfaces made from III–V semiconductors have been employed to show the frequency mixing, including generation of the second-, third- and fourth harmonic, as well as four-wave mixing and six-wave mixing nonlinear processes.[11] Such a metasurface consists of a periodic array of cylindrical resonators with three layers: the top is an SiO_x etch mask that is an exposed hydrogen silsesquioxane photoresist, the middle is the

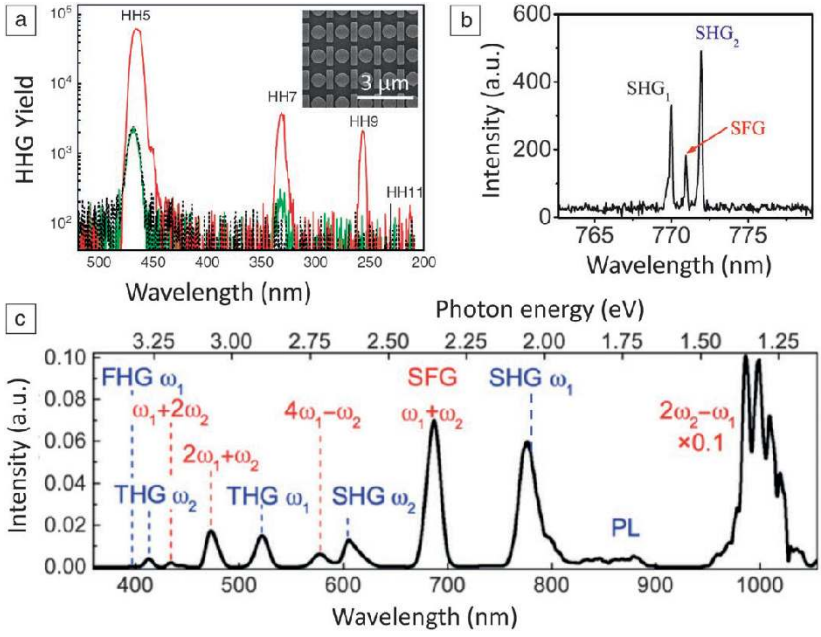

Figure 6. High-harmonic generation in semiconductor metasurfaces. (a) Spectra of the high harmonics generated from a Si metasurface, demonstrating the possibility to generate harmonics ranging from fifth (HH5) to 11th (HH11) order when the excitation pulses centered at λ = 2320 nm are polarized parallel (red line) and perpendicular (green line) to the nanobars on the metasurface (shown by the scanning electron microscope picture in the inset). The dotted black line is the high-harmonic spectrum from the unpatterned Si film for comparison.[72] (b) Frequency up-conversion spectrum obtained from a GaSe metasurface when pumped by two continuous wave lasers at wavelengths of 1540.0 nm (laser$_1$) and 1543.9 nm (laser$_2$), showing second-harmonic generation (SHG$_1$ from laser$_1$ and SHG$_2$ from laser$_2$) and sum-frequency mixing (SFG from laser$_1$ and laser$_2$) peaks. (c) Spectrum of frequency mixing exhibiting eleven peaks originating from seven different nonlinear processes when two optical beams at wavelengths λ_1 ~ 1.57 μm and λ_2 ~ 1.24 μm are used to simultaneously pump a GaAs metasurface. Blue labels: harmonic generation and photoluminescence (PL) arising from two-photon absorption with one pump beam. Red labels: frequency mixing that involves both pump beams.[11] Note: HHG, high-harmonic generation; THG, third-harmonic generation; FHG, fourth-harmonic generation; ω_1, frequency corresponding to λ_1; ω_2, frequency corresponding to λ_2.

GaAs layer, and the bottom layer is the oxide $(Al_{0.85}Ga_{0.15})_2O_3$.[11] When two femtosecond pump beams simultaneously pump the GaAs metasurface with wavelengths overlapping with the magnetic and electric dipole resonances, the nonlinear generation of 11 new frequencies with spectra spanning from ultraviolet to near-infrared can be detected (Figure 6c). Due to the small feature size of the resonators, the metasurface relaxes phase-matching conditions, which leads to the possibility of the generation of a few different nonlinear processes at the same time. The newly generated frequencies can be divided into two groups. The first group relies only on one beam—SHG, THG, fourth-harmonic generation, and photoluminescence. The second group of signals relies on two pump beams—sum-frequency mixing (SFG), six-wave mixing, and three peaks that correspond to four-wave mixing processes.

Nonlinear metadevices

Metasurfaces emerged as a two-dimensional (2D) version of metamaterials with properties beyond those described by effective or averaged parameters. Being structured on the subwavelength scale, metasurfaces substantially extended the concept of diffraction gratings, and they became a paradigm for engineering electromagnetic space and controlling the propagation of waves. The current research agenda is to achieve tunable, switchable, nonlinear, and sensing functionalities of flat optics, creating a platform for the emerging field of planar metadevices, which we define as devices with unique and useful functionalities realized by structuring of functional matter on the subwavelength scale. Here, we summarize and discuss several experimentally demonstrated nonlinear metadevices engaging nonlinear response of their subwavelength components.

Wang et al.[9] suggested a general approach for engineering the wavefront of parametric waves of arbitrary complexity generated by a nonlinear metasurface. They designed all-dielectric nonlinear metasurfaces with a highly efficient wavefront control of the third-harmonic field, and demonstrated the generation of nonlinear beams at a designed angle and the generation of nonlinear focusing vortex beams, as shown in **Figure 7**a–b. Their nonlinear metasurfaces produced phase gradients over a full 0–2π phase range. Figure 7a shows a directionality diagram (back-focal plane image) of the forward

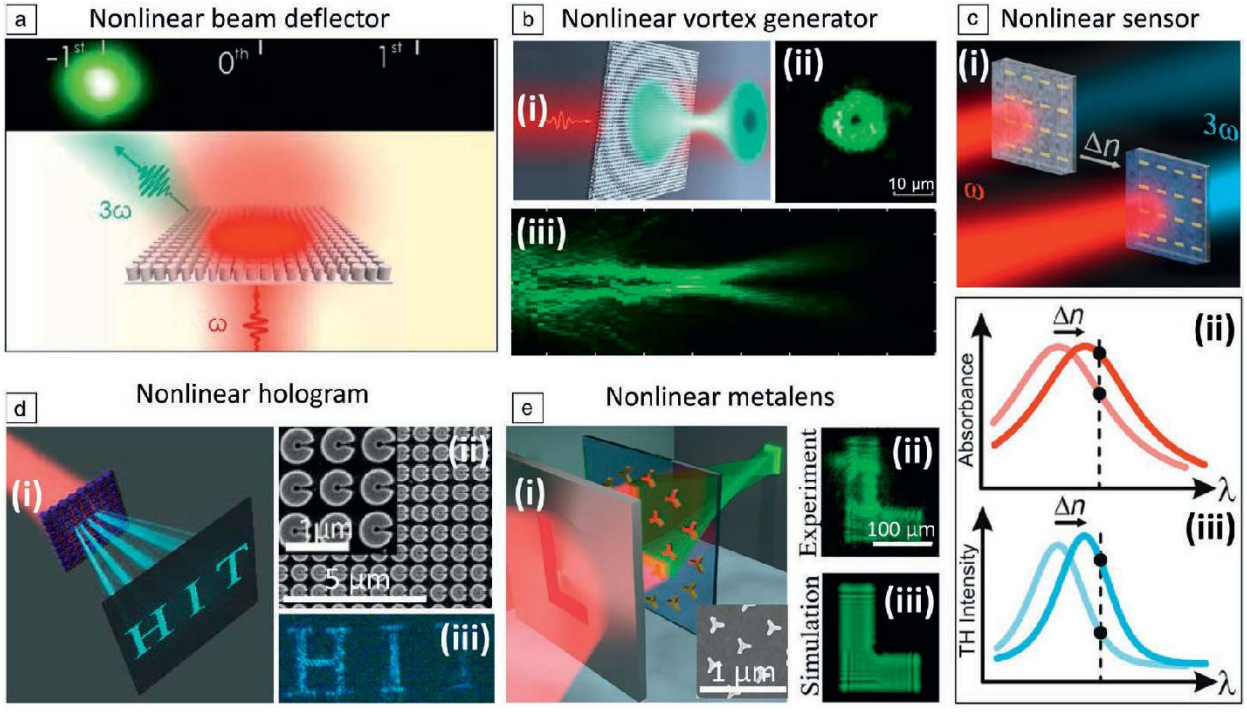

Figure 7. Examples of nonlinear metadevices exploring spatial control of nonlinear fields with metasurfaces. (a) Nonlinear beam-deflector metasurface.[9] (Bottom) Schematic of the nonlinear beam deflector showing the excitation at frequency ω and the deflected third-harmonic generation (THG) at frequency 3ω. Top: Directionality diagram (back-focal plane image) of the forward third-harmonic field. (b) (i) Nonlinear vortex beam generator.[9] Cross sections of a generated donut-shaped vortex beam taken (ii) perpendicular to the optical axis and (iii) along the optical axis of the beam. (c) (i) Principle of linear and nonlinear metasurface-based sensing. (ii) Influence of the linear sensing mechanism on absorbance. (iii) Influence of nonlinear sensing scheme on THG. The dashed lines indicate the wavelength for which the strongest signal change could be observed in the demonstrated sensing scheme.[73] (d) Nonlinear metasurface hologram. (i) Scheme of the setup. (ii, inset) Scanning electron microscope images of the C-shaped Si metasurface. (iii) Experimentally obtained holographic image for a wavelength of 483 nm.[74] (e) (i) Schematic concept of a nonlinear metalens, with L-shaped apertures imaged on a screen with the help of the nonlinear metalens consisting of triangular nanoantennas. (ii) Measured second-harmonic generation distribution in image plane compared to (iii) the corresponding simulation.[77] Note: ω, frequency of exciting light; TH, third harmonic; *n*, index of refraction; λ, wavelength.

third-harmonic field. A total of 92% of the third-harmonic field is directed into the designed angle $\theta = 5.6°$.

The idea to employ nonlinear metasurfaces for sensing has been suggested as an example of application of plasmonic metasurfaces.[73] A refractive index difference, Δn, in the environment of the metasurface causes a shift of its resonance frequency. In nonlinear sensing, the resonance is driven at frequency ω, and the resonantly enhanced third harmonic at frequency 3ω serves as the sensor signal (Figure 7c). Because of the nonlinear conversion process, one can observe a larger sensitivity to a local change in the refractive index as compared to the commonly used linear localized surface plasmon resonance sensing.[73] Furthermore, simultaneous detection of linear and nonlinear signals allows comparison of both methods, providing further insight into the working principle of this sensor. While the signal-to-noise ratio is comparable, nonlinear sensing gives about seven times higher relative signal changes, which could improve applications, for example, for refractive index or single molecule sensing.

Nonlinear holographic metasurfaces have been intensively studied due to their potential in practical applications.[13,74,75] Gao et al.[74] demonstrated a novel mechanism for nonlinear holographic metasurfaces. In contrast to conventional studies, their all-dielectric metasurface is composed of C-shaped Si nanoantennas. The incident laser is enhanced by their fundamental resonance, whereas the generated THG signals are redistributed to the air gap region via the higher order resonance, significantly reducing the absorption loss at short wavelengths and resulting in an enhancement factor as high as 230. After introducing abrupt phase changes from 0 to 2π to the C elements, high-efficiency THG holograms have been experimentally generated with the Si metasurface (Figure 7d).

Another attractive application of metasurfaces is imaging by planar metalenses, which enables device miniaturization and aberration correction compared to conventional optical microlens systems. An abrupt phase change of light at metasurfaces provides high flexibility in wave manipulation without the need of accumulation of propagating phase through dispersive materials.[76] With nonlinear responses, optical functionalities of metalenses are anticipated to be further enriched, leading to completely new application areas. Schlickriede et al.[77] have demonstrated an ultrathin nonlinear metalens using SHG from gold meta-atoms with threefold rotational symmetry. The desired phase profile for a metalens was obtained by a nonlinear Pancharatnam–Berry phase (see Reference 77) that is governed by the meta-atom orientation angle and the spin state of the fundamental wave. For a near-infrared Gaussian laser beam, the authors realized the spin-dependent focusing effect of SHG waves at both real and virtual focal planes. Furthermore, they showed that objects illuminated by near infrared light can be imaged at a visible wavelength based on the SHG process at the metalens, as shown in Figure 7e. The concept of a nonlinear metalens not only inspires new imaging technologies, but also provides a novel platform for generating and modulating nonlinear optical waves.

Several groups have studied optical switching by employing two-photon absorption,[78] carrier injection,[79] intensity-dependent refractive index of chalcogenide glass,[80] and strong absorption saturation.[81] In particular, Shcherbakov et al.[79] realized an ultrafast tunable metasurface consisting of subwavelength GaAs nanoparticles supporting Mie-type resonances in the near infrared. Using transient reflectance spectroscopy, they demonstrated a picosecond-scale absolute reflectance modulation of up to 0.35 at the magnetic dipole resonance of the metasurfaces and a spectral shift of the resonance by 30 nm, both achieved at unprecedentedly low pump fluence of less than 400 $\mu J\ cm^{-2}$. Their findings enable a versatile tool for ultrafast and efficient control of light using light. However, practical ultrafast and efficient metadevices based on these effects are yet to be demonstrated.

Summary and outlook

For efficient nonlinear processes in optics, engineering the nonlinear properties of media becomes an important task. The well-known approach for engineering nonlinear optical properties is the quasi-phase-matching scheme for enhancing second-order processes such as SHG, based on binary periodic polling of natural crystals, which is equivalent to a discrete phase change of the nonlinear polarization. Continuous control of the phase of the nonlinear susceptibility can greatly enhance flexibility in the design; the latter becomes possible with metamaterials. Thus, nonlinear metamaterials have fundamental significance in nonlinear optics for tailored nonlinearities, as they provide novel degrees of freedom in the design of optical materials with nontrivial nonlinear response.

Metasurfaces, assembled from 2D arrays of optical resonators, do not require any phase-matching condition, and they rely on local enhancement of both electric and magnetic fields, so resonances play an important role in the physics of nonlinear metasurfaces. In this article, we have outlined the most recent advances in the emerging field of nonlinear metasurfaces largely driven by dielectric nanostructures supporting Mie-type and guided-mode resonances. This is a rapidly developing field with great potential for applications in new types of beam control devices, frequency conversion with flat optics, next-generation displays, and quantum processing. Subwavelength confinement of local electromagnetic fields in resonant high-index dielectric photonic nanostructures due to individual Mie and collective Fano resonances, as well as interference physics of the different types of bound states in the continuum, can boost many effects in nonlinear optics, thus offering novel opportunities for subwavelength control of light at the nanoscale for components of future nonlinear metadevices. These are defined as devices having unique and useful functionalities through structuring functional matter on the subwavelength scale. An open challenge in this respect is set by the limited product of Q factor and bandwidth, which restricts the utilization of ultrashort pulses for exciting the nonlinear response of metasurfaces with ultrahigh-Q factors, due to the finite bandwidth of the resonant enhancement.

However, strong non-perturbative nonlinear effects might introduce new solution strategies in this direction.

Further developments are expected from introducing new materials for realizing nonlinear metasurfaces. As one example, the nonlinearity of Si-based devices is limited to a third-order nonlinearity due to the crystal symmetry of Si. Hence, the nonlinear efficiencies remain relatively low, which hinders their practical applications with low-power lasers. However, combining Si metasurfaces with 2D GaSe flakes can assist high-efficiency second-order nonlinear processes, including SHG and SFG.[82] The obtained SHG from the Si–GaSe metasurface is approximately two orders of magnitude stronger than THG from the bare Si metasurface. In addition, the resonant field enhancement and GaSe-induced strong second-order nonlinearity, make it possible to observe SFG as well. Besides the hybridization of dielectric metasurfaces with various types of 2D materials,[82] the direct nanopatterning of strongly nonlinear atomic membranes is a future attractive direction to develop atomically thin nonlinear metasurfaces.[83,84] Other prospective future developments of the field can be associated with novel directions such as nonlinear topological photonics[66] and realization of quantum effects with flat optics.[85,86] The field of metasurfaces has attracted a great deal of interest for applications of the methods of deep machine learning and global optimization using advanced concepts of physics-inspired theory of neural networks.[87,88]

Another interesting future direction is to control light–matter interactions of organic–inorganic perovskite materials, and their applications in energy harvesting and photonic devices by combining them with resonant dielectric metasurfaces. Organic–inorganic halide perovskites have received extensive interest owing to their high solar conversion efficiencies and low fabrication cost.[89] The combined effects of the two classes of materials, perovskites and metamaterials, can be explored with a design of hybrid structures by patterning perovskites into metasurfaces or placing perovskites on top of a resonant metasurface to control the carrier dynamics and boost the device performance and efficiency for solar cells and photodetectors. Thus, a new approach of engineering perovskites with metasurfaces can bring revolutionary steps toward developing novel linear and nonlinear planar photonic devices.

Nonlinear metasurfaces highlight the importance of optically induced magnetic response of engineering nonmagnetic resonant structures for many applications in optics, including optical sensing, parametric amplification, ultrafast spatial modulation of light, and nonlinear active media, as well as both integrated classical and quantum circuitry and topological photonics, underpinning a new generation of highly efficient flat-optics metadevices.

Acknowledgments

The authors acknowledge useful collaborations and discussions with many colleagues and students. T.P. acknowledges support by the German Federal Ministry of Education and Research (Project IDs 03ZZ0451, 13N14147), the German Research Foundation (Project-ID 398816777—SFB 1375, PE 1524/10-2), and the German Academic Exchange Service (ID 57388353). Y.K. was supported by the Humboldt Foundation, the Australian Research Council (Grant No. DP 200101168), and the Strategic Fund of the Australian National University.

References

1. I. Staude, T. Pertsch, Y.S. Kivshar, *ACS Photonics* **6**, 802 (2019).
2. L. Carletti, D. Rocco, A. Locatelli, C. De Angelis, V.F. Gili, M. Ravaro, I. Favero, G. Leo, M. Finazzi, L. Ghirardini, M. Celebrano, G. Marino, A.V. Zayats, *J. Nanotechnol.* **28**, 114005 (2017).
3. A. Krasnok, M. Tymchenko, A. Alù, *Mater. Today* **21**, 8 (2018).
4. M. Rahmani, G. Leo, I. Brener, A.V. Zayats, S.A. Maier, C. De Angelis, H. Tan, V.F. Gili, F. Karouta, R. Oulton, K. Vora, M. Lysevych, I. Staude, L. Xu, A.E. Miroshnichenko, C. Jagadish, D.N. Neshev, *Opto-Electron. Adv.* **1**, (10), 180021 (2018).
5. B. Sain, C. Meier, T. Zentgraf, *Adv. Photonics* **1**, 024002 (2019).
6. C. Zou, J. Sautter, F. Setzpfandt, I. Staude, *J. Phys. D Appl. Phys.* **52**, 373002 (2019).
7. M.R. Shcherbakov, F. Eilenberger, I. Staude, *J. Appl. Phys.* **126**, 085705 (2019).
8. C. Gigli, G. Marino, A. Borne, P. Lalanne, G. Leo, *Front. Phys.* **7**, 221 (2019).
9. L. Wang, S. Kruk, K. Koshelev, I. Kravchenko, B. Luther-Davies, Y. Kivshar, *Nano Lett.* **18**, 3978 (2018).
10. K. Koshelev, Y. Tang, K. Li, D.-Y. Choi, G. Li, Y. Kivshar, *ACS Photonics* **6**, 1639 (2019).
11. S. Liu, P.P. Vabishchevich, A. Vaskin, J.L. Reno, G.A. Keeler, M.B. Sinclair, I. Staude, I. Brener, *Nat. Commun.* **9**, 2507 (2018).
12. C. Schlickriede, S. Kruk, L. Wang, B. Sain, Y. Kivshar, T. Zentgraf, "Nonlinear Dielectric Metalenses: Imaging and Higher-Order Correlations," in *Conference on Lasers and Electro-Optics*, OSA Technical Digest (Optical Society of America, Washington, DC, 2019), paper JTh5B.10.
13. E. Almeida, O. Bitton, Y. Prior, *Nat. Commun.* **7**, 12533 (2016).
14. A.I. Kuznetsov, A.M. Miroshnichenko, M.L. Brongersma, Y.S. Kivshar, B. Lukyanchuk, *Science* **354**, aag2472 (2016).
15. I. Staude, J. Schilling, *Nat. Photonics* **11**, 274 (2017).
16. S. Kruk, Y.S. Kivshar, *ACS Photonics* **4**, 2638 (2017).
17. M.F. Limonov, M.V. Rybin, A.N. Poddubny, Y.S. Kivshar, *Nat. Photonics* **11**, 543 (2017).
18. B. Hopkins, A.N. Poddubny, A.E. Miroshnichenko, Y.S. Kivshar, *Phys. Rev. A* **88**, 053819 (2013).
19. S. Liu, M.R. Sinclair, T.S. Mahony, Y.C. Jun, S. Campione, J. Ginn, D.A. Bender, J. Wendt, J.F. Inglefeld, P.G. Clem, J.B. Wright, I. Brener, *Optica* **1**, 250 (2014).
20. S.S. Wang, R. Magnusson, J.S. Bagby, M.G. Moharam, *J. Opt. Soc. Am. A* **7**, 1470 (1990).
21. C.W. Hsu, B. Zhen, A.D. Stone, J.D. Joannopoulos, M. Soljacic, *Nat. Rev. Mater.* **1**, 16048 (2016).
22. A. Kodigala, T. Lepetit, Q. Gu, B. Bahari, Y. Fainman, B. Kante, *Nature* **541**, 196 (2017).
23. M. Rybin, Y.S. Kivshar, *Nature* **541**, 165 (2017).
24. K. Koshelev, S. Lepeshov, M. Liu, A. Bogdanov, Y.S. Kivshar, *Phys. Rev. Lett.* **121**, 193903 (2018).
25. S. Campione, S. Liu, L.I. Basilio, L.K. Warne, W.L. Langston, T.S. Luk, J.R. Wendt, J.L. Reno, G.A. Keeler, I. Brener, M.B. Sinclair, *ACS Photonics* **3**, 2362 (2016).
26. A. Tittl, A. Leitis, M. Liu, F. Yesilkoy, D.-Y. Choi, D.N. Neshev, Y.S. Kivshar, H. Altug, *Science* **360**, 1105 (2018).
27. L. Fonda, *Ann. Phys.* **22**, 123 (1963).
28. Z. Liu, Y. Xu, Y. Lin, J. Xiang, T. Feng, Q. Cao, J. Li, S. Lan, J. Liu, *Phys. Rev. Lett.* **123**, 253901 (2019).
29. A. Leitis, A. Tittl, M. Liu, B.H. Lee, M.B. Gu, Y.S. Kivshar, H. Altug, *Sci. Adv.* **5**, eaaw2871 (2019).
30. C. Cui, C. Zhou, S. Yuan, X. Qiu, L. Zhu, Y. Wang, Y. Li, J. Song, Q. Huang, Y. Wang, C. Zeng, J. Xia, *ACS Photonics* **5**, 4074 (2018).
31. M.W. Klein, C. Enkrich, M. Wegener, S. Linden, *Science* **313**, 502 (2006).
32. B. Canfield, H. Husu, J. Laukkanen, B. Bai, M. Kuittinen, J. Turunen, M. Kauranen, *Nano Lett.* **7**, 1251 (2007).
33. J. Zhang, K.F. MacDonald, N.I. Zheludev, *Light Sci. Appl.* **2**, e96 (2013).
34. L. Carletti, A. Locatelli, O. Stepanenko, G. Leo, C. De Angelis, *Opt. Express* **23**, 26544 (2015).
35. C.R. Ma, J.H. Yan, P. Liu, Y.M. Wei, G.W. Yang, *J. Mater. Chem. C* **4**, 6063 (2016).
36. V.F. Gili, L. Carletti, A. Locatelli, D. Rocco, M. Finazzi, L. Ghirardini, I. Favero, C. Gomez, A. Lemaître, M. Celebrano, C. De Angelis, G. Leo, *Opt. Express* **24**, 15965 (2016).
37. R. Camacho-Morales, M. Rahmani, S. Kruk, L. Wang, L. Xu, D.A. Smirnova, A. Solntsev, A.E. Miroshnichenko, H.H. Tan, F. Karouta, S. Naureen, K. Vora, L. Carletti, C. De Angelis, C. Jagadish, Y.S. Kivshar, D.N. Neshev, *Nano Lett.* **16**, 7191 (2016).

38. L. Ghirardini, L. Carletti, V. Gili, G. Pellegrini, L. Duo, M. Finazzi, D. Rocco, A. Locatelli, C. De Angelis, I. Favero, M. Ravaro, G. Leo, A. Lemaitre, M. Celebrano, *Opt. Lett.* **42**, 559 (2017).
39. M. Semmlinger, M.L. Tseng, J. Yang, M. Zhang, C. Zhang, W.-Y. Tsai, D.P. Tsai, P. Nordlander, N.J. Halas, *Nano Lett.* **18** (9), 5738 (2018).
40. L. Carletti, G. Marino, L. Ghirardini, V. F Gili, D. Rocco, I. Favero, A. Locatelli, A.V. Zayats, M. Celebrano, M. Finazzi, G. Leo, C. De Angelis, D.N. Neshev, *ACS Photonics* **5**, 4386 (2019).
41. J. Sautter, L. Xu, A. E Miroshnichenko, M. Lysevych, I. Volkovskaya, D. A Smirnova, R. Camacho-Morales, K.Z. Kamali, F. Karouta, K. Vora, H.H. Tan, M. Kauranen, I. Staude, C. Jagadish, D. N Neshev, M. Rahmani, *Nano Lett.* **19**, 3905 (2019).
42. S. Liu, M.B. Sinclair, S. Saravi, G.A. Keeler, Y. Yang, J. Reno, G.M. Peake, F. Setzpfandt, I. Staude, T. Pertsch, I. Brener, *Nano Lett.* **16**, 5426 (2016).
43. P.P. Vabishchevich, S. Liu, M.B. Sinclair, G.A. Keeler, G.M. Peake, I. Brener, *ACS Photonics* **5**, 1685 (2018).
44. F.J. Löchner, A.N. Fedotova, S. Liu, G.A. Keeler, G.M. Peake, S. Saravi, M.R. Shcherbakov, S. Burger, A.A. Fedyanin, I. Brener, T. Pertsch, F. Setzpfandt, I. Staude, *ACS Photonics* **5**, 1786 (2018).
45. G. Marino, C. Gigli, D. Rocco, A. Lemaître, I. Favero, C. De Angelis, G. Leo, *ACS Photonics* **6**, 1226 (2019).
46. C. Gigli, G. Marino, S. Suffit, G. Patriarche, G. Beaudoin, K. Pantzas, I. Sagnes, I. Favero, G. Leo, *J. Opt. Soc. Am. B* **36**, E55 (2019).
47. K. Frizyuk, I. Volkovskaya, D. Smirnova, A. Poddubny, M. Petrov, *Phys. Rev. B* **99**, 075425 (2019).
48. D. Lehr, J. Reinhold, I. Thiele, H. Hartung, K. Dietrich, C. Menzel, T. Pertsch, E.-B. Kley, A. Tünnermann, *Nano Lett.* **15**, 1025 (2015).
49. C. Ma, J. Yan, Y. Wei, P. Liu, G. Yang, *J. Mater. Chem. C* **5**, 4810 (2017).
50. F. Timpu, N.R. Hendricks, M. Petrov, S. Ni, C. Renaut, H. Wolf, L. Isa, Y. Kivshar, R. Grange, *Nano Lett.* **17**, 5381 (2017).
51. F. Timpu, J. Sendra, C. Renaut, L. Lang, M. Timofeeva, M.T. Buscaglia, V. Buscaglia, R. Grange, *ACS Photonics* **6**, 545 (2019).
52. L. Carletti, C. Li, J. Sautter, I. Staude, C. De Angelis, T. Li, D.N. Neshev, *Opt. Express* **27**, 3339127 (2019).
53. A. Fedotova, M. Younesi, J. Sautter, M. Steinert, R. Geiss, T. Pertsch, I. Staude, F. Setzpfandt, "Second-Harmonic Generation in Lithium Niobate Metasurfaces," in *2019 Conference on Lasers and Electro-Optics Europe and European Quantum Electronics Conference*, OSA Technical Digest (Optical Society of America, Washington, DC, 2019), paper ef_1_2.
54. C.R. Ma, J.H. Yan, Y.M. Wei, G.W. Yang, *Nanotechnology* **27**, 425206 (2016).
55. J. Cambiasso, G. Grinblat, Y. Li, A. Rakovich, E. Cortes, S.A. Maier, *Nano Lett.* **17**, 1219 (2017).
56. S.V. Makarov, M.I. Petrov, U. Zywietz, V. Milichko, D. Zuev, N. Lopanitsyna, A. Kuksin, I. Mukhin, G. Zograf, E. Ubyivovk, D.A. Smirnova, S. Starikov, B.N. Chichkov, Y.S. Kivshar, *Nano Lett.* **17**, 3047 (2017).
57. J. Bar-David, U. Levy, *Nano Lett.* **19** (2), 1044 (2019).
58. M.R. Shcherbakov, D.N. Neshev, B. Hopkins, A.S. Shorokhov, I. Staude, E.V. Melik-Gaykazyan, M. Decker, A.A. Ezhov, A.E. Miroshnichenko, I. Brener, A.A. Fedyanin, Y.S. Kivshar, *Nano Lett.* **14**, 6488 (2014).
59. G. Grinblat, Y. Li, M.P. Nielsen, R.F. Oulton, S.A. Maier, *Nano Lett.* **16**, 4635 (2016).
60. E.V. Melik-Gaykazyan, M.R. Shcherbakov, A.S. Shorokhov, I. Staude, I. Brener, D.N. Neshev, Y.S. Kivshar, A.A. Fedyanin, *Philos. Trans. R. Soc. A* **375**, 20160281 (2017).
61. T. Shibanuma, G. Grinblat, P. Albella, S.A. Maier, *Nano Lett.* **17**, 2647 (2017).
62. Y. Yang, W. Wang, A. Boulesbaa, I.I. Kravchenko, D.P. Briggs, A. Puretzky, D. Geohegan, J. Valentine, *Nano Lett.* **15**, 7388 (2015).
63. W. Tong, C. Gong, X. Liu, S. Yuan, Q. Huang, J. Xia, Y. Wang, *Opt. Express* **24**, 19661 (2016).
64. S.V. Makarov, A.N. Tsypkin, T.A. Voytova, V.A. Milichko, I.S. Mukhin, A.V. Yulin, S.E. Putilin, M.A. Baranov, A.E. Krasnok, I.A. Morozov, P.A. Belov, *Nanoscale* **8**, 17809 (2016).
65. S. Chen, M. Rahmani, K.F. Li, A. Miroshnichenko, T. Zentgraf, G. Li, D. Neshev, S. Zhang, *ACS Photonics* **5**, 1671 (2018).
66. D. Smirnova, S. Kruk, D. Leykam, E. Melik-Gaykazyan, D.-Y. Choi, Y. Kivshar, *Phys. Rev. Lett.* **123**, 103901 (2019).
67. M.R. Shcherbakov, A.S. Shorokhov, D.N. Neshev, B. Hopkins, I. Staude, E.V. Melik-Gaykazyan, A.A. Ezhov, A.E. Miroshnichenko, I. Brener, A.A. Fedyanin, Y.S. Kivshar, *ACS Photonics* **2**, 578 (2015).
68. A.S. Shorokhov, E.V. Melik-Gaykazyan, D.A. Smirnova, B. Hopkins, K.E. Chong, D.Y. Choi, M.R. Shcherbakov, A.E. Miroshnichenko, D.N. Neshev, A.A. Fedyanin, Y.S. Kivshar, *Nano Lett.* **16**, 4857 (2016).
69. M.K. Kroychuk, D.F. Yagudin, A.S. Shorokhov, D.A. Smirnova, I.I. Volkovskaya, M.R. Shcherbakov, G. Shvets, Y.S. Kivshar, A.A. Fedyanin, *Adv. Opt. Mater.* **7**, 1900447 (2019).
70. G. Vampa, H. Fattahi, J. Vuckovic, F. Krausz, *Nat. Photonics* **11**, 210 (2017).
71. G. Ndabashimiye, S. Ghimire, M. Wu, D.A. Browne, K.J. Schafer, M.B. Gaarde, D.A. Reis, *Nature* **534**, 520 (2016).
72. H. Liu, C. Guo, G. Vampa, J.L. Zhang, T. Sarmiento, M. Xiao, P.H. Bucksbaum, J. Vučkovic, S. Fan, D.A. Reis, *Nat. Phys.* **14**, 1006 (2018).
73. M. Mesch, B. Metzger, M. Hentschel, H. Giessen, *Nano Lett.* **16**, 3155 (2016).
74. Y. Gao, Y. Fan, Y. Wang, W. Yang, Q. Song, S. Xiao, *Nano Lett.* **18** (12), 8054 (2018).
75. B. Reineke, B. Sain, R. Zhao, L. Carletti, B. Liu, L. Huang, C. De Angelis, T. Zentgraf, *Nano Lett.* **19**, 6585 (2019).
76. P. Lalanne, S. Astilean, P. Chavel, E. Cambril, H. Launois, *J. Opt. Soc. Am. A* **16**, 1143 (1999).
77. C. Schlickriede, N. Waterman, B. Reineke, P. Georgi, G. Li, S. Zhang, T. Zentgraf, *Adv. Mat.* **30**, 1703843 (2018).
78. M.R. Shcherbakov, P.P. Vabishchevich, A.S. Shorokhov, K.E. Chong, D.Y. Choi, I. Staude, A.E. Miroshnichenko, D.N. Neshev, A.A. Fedyanin, Y.S. Kivshar, *Nano Lett.* **15**, 6985 (2015).
79. M.R. Shcherbakov, S. Liu, V.V. Zubyuk, A. Vaskin, P.P. Vabishchevich, G. Keeler, T. Pertsch, T.V. Dolgova, I. Staude, I. Brener, A.A. Fedyanin, *Nat. Commun.* **8**, 17 (2017).
80. Y. Xu, J. Sun, J. Frantz, M.I. Shalaev, W. Walasik, A. Pandey, J.D. Myers, R.Y. Bekele, A. Tsukernik, J.S. Sanghera, N.M. Litchinitser, *Opt. Express* **26**, 30930 (2018).
81. V.V. Zubyuk, P.P. Vabishchevich, M.R. Shcherbakov, A.S. Shorokhov, A.N. Fedotova, S. Liu, G. Keeler, T.V. Dolgova, I. Staude, I. Brener, A.A. Fedyanin, *ACS Photonics* **6**, 2797 (2019).
82. Q. Yuan, L. Fang, H. Fang, J. Li, T. Wang, W. Jie, J. Zhao, X. Gan, *ACS Photonics* **6**, 2252 (2019).
83. A. Dasgupta, J. Gao, X. Yang, *Nano Lett.* **19**, 6511 (2019).
84. F.J.F. Löchner, R. Mupparapu, M. Steinert, A. George, Z. Tang, A. Turchanin, T. Pertsch, I. Staude, F. Setzpfandt, *Opt. Express* **27**, 35475 (2019).
85. K. Wang, J.G. Titchener, S.S. Kruk, L. Xu, H.-P. Chung, M. Parry, I.I. Kravchenko, Y.-H. Chen, A.S. Solntsev, Y.S. Kivshar, D.N. Neshev, A.A. Sukhorukov, *Science* **361**, 1104 (2018).
86. G. Marino, A.S. Solntsev, L. Xu, V.F. Gili, L. Carletti, A.N. Poddubny, M. Rahmani, D.A. Smirnova, H. Chen, A. Lemaître, G. Zhang, A.V. Zayats, C. De Angelis, G. Leo, A.A. Sukhorukov, D.N. Neshev, *Optica* **6**, 1416 (2019).
87. C.C. Nadell, B. Huang, J.M. Malof, W.J. Padilla, *Opt. Express* **27**, 27523 (2019).
88. J. Jiang, J.A. Fan, *Nano Lett.* **19**, 5366 (2019).
89. A.S. Berestennikov, P.M. Voroshilov, S.V. Makarov, Y.S. Kivshar, *Appl. Phys. Rev.* **6**, 031307 (2019). □

Thomas Pertsch is a professor at the Friedrich Schiller University Jena, Germany. He received his Diploma degree in electrical engineering in 1996 from the Technical University Dresden, Germany, and Rensselaer Polytechnic Institute, and his PhD degree in physics from Friedrich Schiller University Jena, Germany, in 2003. His research interests include nano- and quantum optics, metamaterials, and nanophotonics. He is a member of the Abbe Center of Photonics, as well as a Fellow of The Optical Society and the Max Planck School of Photonics. Pertsch can be reached by email at thomas.pertsch@uni-jena.de.

Yuri Kivshar is a distinguished professor at The Australian National University, Australia. He received his PhD degree in 1984 from the USSR Academy of Science, Ukraine. From 1988 to 1993, he worked at several international research centers, and since 1993, he has been at the Nonlinear Physics Center, The Australian National University, Australia. His research interests include nonlinear physics, metamaterials, and nanophotonics. He is a Fellow of the Australian Academy of Science, The Optical Society, the American Physical Society, (SPIE), the International Society for Optics and Photonics, and the Institute of Physics. His awards include the Pnevmatikos Prize in Nonlinear Science, the Thomas Rankin Lyle Medal, the Lebedev Medal, the State Prize in Science and Technology, the Harrie Massey Medal, the Humboldt Research Award, and the SPIE Mozi Award. Kivshar can be reached by email at ysk124@physics.anu.edu.au.